Polymer-Decorated Anisotropic Silica Nanotubes with Combined Shape and Surface Properties for Guest Delivery

Guo Liang Li,[1,3]* Jinglei Hu,[2]* Hongqiang Wang,[4] Christine Pilz-Allen,[3] Junpeng Wang,[1] Tao Qi,[1] Helmuth Möhwald[3] and Dmitry G. Shchukin[4]

[1]National Engineering Laboratory for Hydrometallurgical Cleaner Production Technology, Institute of Process Engineering, Chinese Academy of Sciences, Beijing 100190, P. R. China

[2]Kuang Yaming Honors School, Nanjing University, 210093, Nanjing, P. R. China

[3]Max Planck Institute of Colloids and Interfaces, Wissenschaftspark Golm, Am Mühlenberg 1, 14476 Potsdam, Germany

[4]Stephenson Institute for Renewable Energy, Department of Chemistry, University of Liverpool, Crown Street, Liverpool, L69 7ZD, United Kingdom

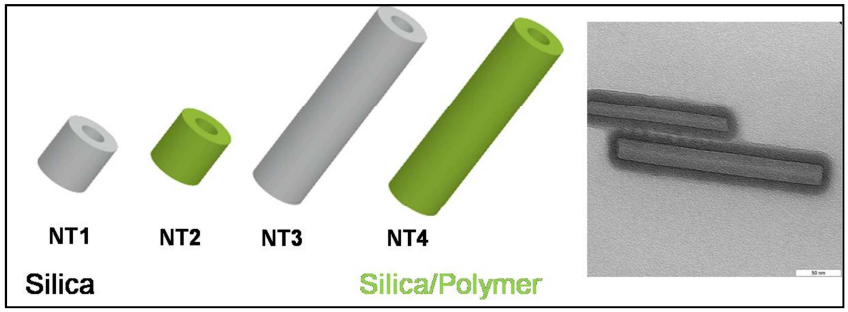

* Corresponding Authors

Email: glli@ipe.ac.cn (G. Li)
Email: hujinglei@nju.edu.cn (J. Hu)

Abstract

We report on amphiphilic diblock copolymer-decorated anisotropic silica nanotubes with defined dual functions of shape and surface properties in one nanocontainer. Amphiphilic poly(lactic acid)-*block*-poly(ethylene glycol) (PLA-*b*-PEG) diblock copolymers are covalently grafted to the surface of mesoporous silica nanotubes via silane chemistry and esterification. The released percentage of probe molecules from the resultant silica-*g*-(PLA-*b*-PEG) hybrid nanocontainer is around 40% over a release time of 48 hours, in contrast to 90% from bare silica nanotubes prior to surface modification. The diblock copolymer-decorated anisotropic nanocontainers with large aspect ratio lead to enhanced viability of NIH 3T3 fibroblast cells. A theoretical model based on the free energy cost for cell membranes to encapsulate nanocontainers is utilized to understand the cytotoxicity. This work demonstrates that the release dynamics of the active molecules and the interaction of hybrid nanocontainers with cell membranes can be regulated by the synergistic effect of nanocontainer shape and surface properties.

Introduction

Nanocontainers are of great interest, if they exhibit sophisticated hollow structures, functional permeable shell, and provide diverse applications in medicine, catalysis, energy storage and as a component of self healing materials.[1-7] A variety of organic containers with regulated size and size distribution, including liposomes, dendrimers, colloidosomes, micelles and peptides have been developed in the past years.[8-15] In addition to the size, functional surfaces of nanocontainers to achieve biocompatibility or targeting properties are essential to improve the efficacy and specificity of active molecules in delivery systems.[16-23] Furthermore, a sophisticated geometry is important to affect the permeation barriers for efficient therapeutics.[13, 24-29] Nonspherical shape with several features such as longer blood circulation time and complex motions under flow conditions is a key design parameter to improve nanocontainers in drug delivery.[27, 30, 31] For instance, wormlike polymer brush as non-spherical nanocarrer can easily internalized by cancer cells.[13] Self-assembly is an efficient strategy for fabrication of one-dimensional nanomaterials with controlled aspect ratios [32-35] as well as stimuli-responsive properties for guest delivery.[36] In biological applications, multifunctional features from size, shape and surface properties in one container system are essential. However, integrating dual features of size, anisotropic shape and desirable surface properties in a single nanocontainer is still very challenging, thus the evaluation and theoretical understanding of anisotropic containers is further limited.

Herein we report a facile synthesis of PLA-*block*-PEG diblock copolymer-decorated anisotropic silica nanotubes with a synergistic effect from the shape and surface properties in one container system. The surface grafting of a copolymer on anisotropic silica nanotubes can improve container behaviors in the release dynamics and cellular cytotoxicity tests. Through free energy calculations for the encapsulation of nanocontainers by cell membranes, it shows that the surface grafting of block copolymers on anisotropic nanocontainers maintains the

binding affinity of nanocontainers to cell membranes.

Experimental Section

Materials

Tetraethyl orthosilicate (TEOS), 3-aminopropyltriethoxysilane (APTES), rhodamine 6G, Dulbecco's modified Eagles medium (DMEM), thiazolyl blue tetrazolium bromide (MTT) were purchased from Sigma-Aldrich (Germany). Polyethylene glycol-polyactic acid diblock polymer (PEG(5000)-*B*-PLA(1000)) was purchased from Polysciences, Inc. Brig 58 and cyclohexane (Acros, 99.5%), ammonia solution ($NH_3.H_2O$, Merck, 25%), acetonitrile (Merck, HPLC grade) and dimethylformamide (DMF, Merck, HPLC grade) were used without further purification. The water used in all experiments was prepared in a three-stage Millipore Milli-Q plus 185 purification system and had a resistance higher than 18.2 MΩcm.

Synthesis of Silica-*g*-(PLA-*b*-PEG) Hybrid Nanotubes

Silica nanorods with different aspect ratios were synthesized from nickel-hydrazine/silica core-shell rods.[37, 38] Initially, the nickel hydrazine/silica core-shell nanorods were cleaned repeatedly by isopropanol and ethanol to remove the surfactant. The nanorods were redispersed in THF and collected by precipitation in hexane (volume of hexane to THF is 3:1) followed by centrifugation. Then, 3 mL of 3-aminopropyltriethoxysilane (APTES) and 0.5 mL of diethylamine were introduced dropwise into the nickel hydrazine/silica core-shell rod suspension (45 mL of isopropanol, 5 mg/mL) and stirred at room temperature for 48 h. The nanorods were collected by centrifugation and cleaned repeatedly by ethanol, THF and hexane. The nanotubes with carboxylic acid groups (silica-COOH) were further obtained by a surface reaction between amine groups and succinic anhydride.[39] The silica-NH_2 nanorods were dispersed in the succinic anhydride/DMF solution (0.5 M) and stirred for 48 h at room temperature. The silica-COOH nanotubes were prepared via selective etching of the nickel hydrazine/silica-COOH core-shell rods in HCl solution (1 M), followed by repeated washes with a mixture of ethanol/DI water till a constant pH value.

The surface grafting of PLA-*b*-PEG diblock copolymers onto silica-COOH nanotube surfaces was carried out by an esterification reaction between carboxylic acid groups of silica surfaces and hydroxyl end groups of PLA-*b*-PEG telechelic copolymers.[40] In detail, the suspension of silica-COOH nanotubes (0.4 g) and PLA-*b*-PEG diblock copolymers (0.6 g, 10^{-4} mol, PEG(5000)-*b*-PLA(1000), from Polyscience Inc.) in 20 mL of DMSO was gently stirred at room temperature for 24 h, then a solution of *N, N'*-dicyclohexylcarbodiimide (DCC, 0.0206 g, 10^{-4} mol) and 4-dimethylaminopyridine (DMAP, 0.0018 g, 1.5 x 10^{-5} mol) in DMF was added, and the resultant mixture was stirred at room temperature for three days. The silica-*g*-(PLA-*b*-PEG) hybrid nanotubes were collected by addition of the suspension into diethyl ether under vigorous stirring, followed by vacuum filtration. The nanotubes were then purified by redispersion in THF and precipitated in diethyl ether and were dried in a vacuum oven at room temperature until a constant weight was obtained. The silica-COOH nanotubes and silica-*g*-(PLA-*b*-PEG) hybrid nanotubes with different aspect ratio of 1.12 and 4.72 were obtained by tuning the ratio of hydrazine/nickel during the template growth process.

The grafting density of polymers on silica nanotubes is calculated from TGA analysis by Item 1/Item 2 below.

Item 1 Grafted polymer chains numbers = (grafted polymer amount/Mw) x NA, and **Item 2** Surface areas = $4\Pi r^2$ x Number of the particles.

Where, the grafted polymer amount is from TGA analysis, NA is Avogadro constant, number of particles is calculated by Total volume/($4\ \Pi r^3/3$) = (weight/density)/($4\ \Pi r^3/3$), and r is radius of particle, density of silica-*g*-polymer is calculated to be 1.30 g/cm^3 (SiO_2: 2.2 g/cm^3, PLA-*block*-PEG: 1.2 g/cm^3, 2.2 x 0.31+1.2 x 0.69 =1.30 g/cm^3).

***In vitro* Release Test and Cellular Cytotoxicity Test**

To encapsulate the model probe rhodamine 6G in silica-COOH and silica-*g*-(PLA-*b*-PEG) nanotubes, the Rh6G/nanotube suspension was kept under vacuum overnight to increase the

loading efficiency, then centrifuged and washed with DI water. The supernatant was collected for UV-visible spectra analysis. The loading amount of rhodamine 6G in the nanotubes is given by the difference of the feeding amount and that in the supernatant. The loading capacity was given by the ratio MD = (MD+MT), where MD is the mass of model drug in nanotubes and MT the mass of nanotubes. For the release dynamics, the nanotubes encapsulating rhodamine 6G were added to the dialysis tubing (12-14 KDa), and the release experiments were carried out at room temperature. During the release test, 3 mL of sample solution was taken out after a defined period of time and subjected to UV-visible spectral analysis. Afterwards the sample was placed back into the solution for further release test. The analytical standard curve was obtained by UV-Vis spectroscopy at the wavelength of λ= 275 nm and rhodamine 6G concentrations ranging from 10^{-3} to 10^{-1} mg/mL (Supporting Information, Figure S4).

NIH 3T3 fibroblast cells were seeded 5 times in 24 well plates (1.8 cm^2/well) in 1 mL of cell culture media (DMEM containing 4.5 g/L glucose, 10 vol % of Calf Sera and 10 µg/mL of Gentamicin) at a density of 6 x 10^3 cells per cm^2. The cell counting was carried out with a Casy Cell Counter (Model TT, Company Roche system). In the control experiment, no nanotubes (blank sample) were added into the well. To incubate with nanotubes in cell culture media, cells were first maintained at 37˚C in a humidified atmosphere containing 5% CO_2 for 24 h. Then used media were removed, and media solution was added to the sample at the same tube concentration of 0.1 mg/mL. Each sample was repeated 5 times in 5 wells. Viability of the cells was determined by an MTT assay after 48 h of cell culture. Cells were cultured with 1 mL of fresh medium containing 100 µL MTT stock solution (5 mg MTT/1 mL PBS) in the incubator for 4 h (37^{o}C and 5% CO_2 in the atmosphere). The supernatant was removed and 1 mL of a formazan dissolving solution (99.4 mL DMSO + 10 g SDS + 0.6 mL glacial acetic acid) was added. The solutions were transferred into 96 well plates and the

absorbance at a test wavelength of 570 nm and reference wavelength of 630 nm was immediately read on a microplate reader (Multiscan Ascent, Thermo Fisher).

The size and morphology of the synthesized silica and silica-*g*-(PLA-*b*-PEG) hybrid nanotubes were characterized by scanning electron microscopy (SEM, Zeiss Gemini LEO 1550) and transmission electron microscopy (TEM, Zeiss EM912 Omega). For SEM images, the nanotubes were dispersed in ethanol, dropped onto a clean copper foil on an electron microscope stub, and dried in vacuum at room temperature. For TEM images, the nanotubes dispersed in ethanol were spread onto the surface of a copper grid and then dried in vacuum at room temperature. Fourier-transform infrared (FT-IR) spectroscopy was carried out with a Varian 1000 FT-IR (Scimitar Series) spectrophotometer. The Brunauer-Emmett-Teller (BET) adsorption/desorption isotherm was determined by nitrogen sorption at 77 K using a Micromeritics ASAP 2000 surface area analyzer. The pore size and size distribution were obtained by the DFT method. ^{1}H nuclear magnetic resonance (^{1}HNMR) spectra were measured on a Bruker DPX 400 MHz spectrometer, using $CDCl_3$ as the solvent. Thermogravimetric analysis (TGA) was carried out on a thermogravimetric analyzer (TA Instrument, Model 2050) at a heating rate of 10°C/min in nitrogen. The UV-visible absorption spectra at wavelength from 200 nm to 800 nm were measured on a Varian Cary 50 UV-visible Spectrophotometer.

Results and Discussion

The procedure for the synthesis of anisotropic silica-*g*-(PLA-*b*-PEG) hybrid nanotubes is illustrated in Figure 1A. Initially, silica nanotubes were functionalized via modification of the silica surface with amine groups and carboxylic acid groups by silane chemistry. The as-synthesized silica-COOH nanotubes were then surface-grafted with amphiphilic PLA-*block*-PEG diblock copolymers by esterification between carboxylic acid groups from silica nanotubes and hydroxyl end groups from PLA-*block*-PEG telechelic copolymers. Four types

of silica nanotubes (NT1 and NT3) and silica-*g*-(PLA-*b*-PEG) hybrid nanotubes (NT2 and NT4) were synthesized with different surface functional groups and aspect ratios as shown in Figure 1B. The morphology of nanotubes is shown in Figure 2 from both transmission and scanning electron microscopy (TEM and SEM). Figures 2A and 2B clearly illustrate that the silica-COOH nanotubes (NT1 and NT3, no surface grafting) have well-defined tubular morphologies and different aspect ratios (1.16 and 5.02, respectively). Figure 2C shows that the silica-*g*-(PLA-*b*-PEG) hybrid nanotubes (NT4) exhibit distinctive double-shell structure of the tube walls due to different contrast of the grafted polymers and inorganic silica materials. The wall thickness of silica/polymer hybrid nanotubes is about 10-14 nm (Table 1). The synthesized nanotubes are narrowly dispersed as shown in Figure 2D. The physicochemical properties of the as-synthesized nanotubes with varied geometry and surface properties are summarized in Table 1.

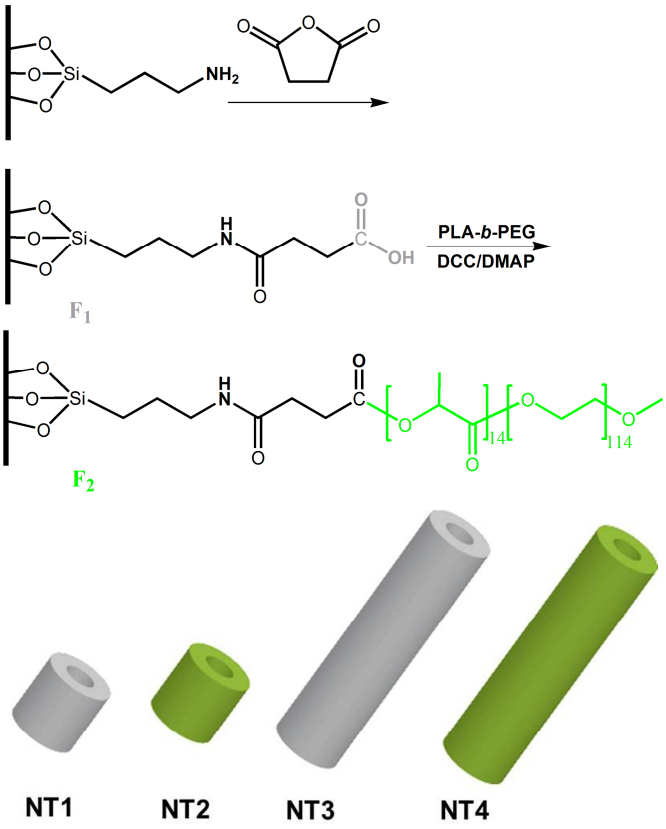

Figure 1 (A) Schematic illustration of the synthesis of amphiphilic diblock copolymer decorated silica nanotubes and (B) four types of functional nanotubes with different aspect

ratio and surface properties (NT1 and NT3 are bare silica nanotubes, NT2 and NT4 are silica/polymer hybrid nanotubes, respectively).

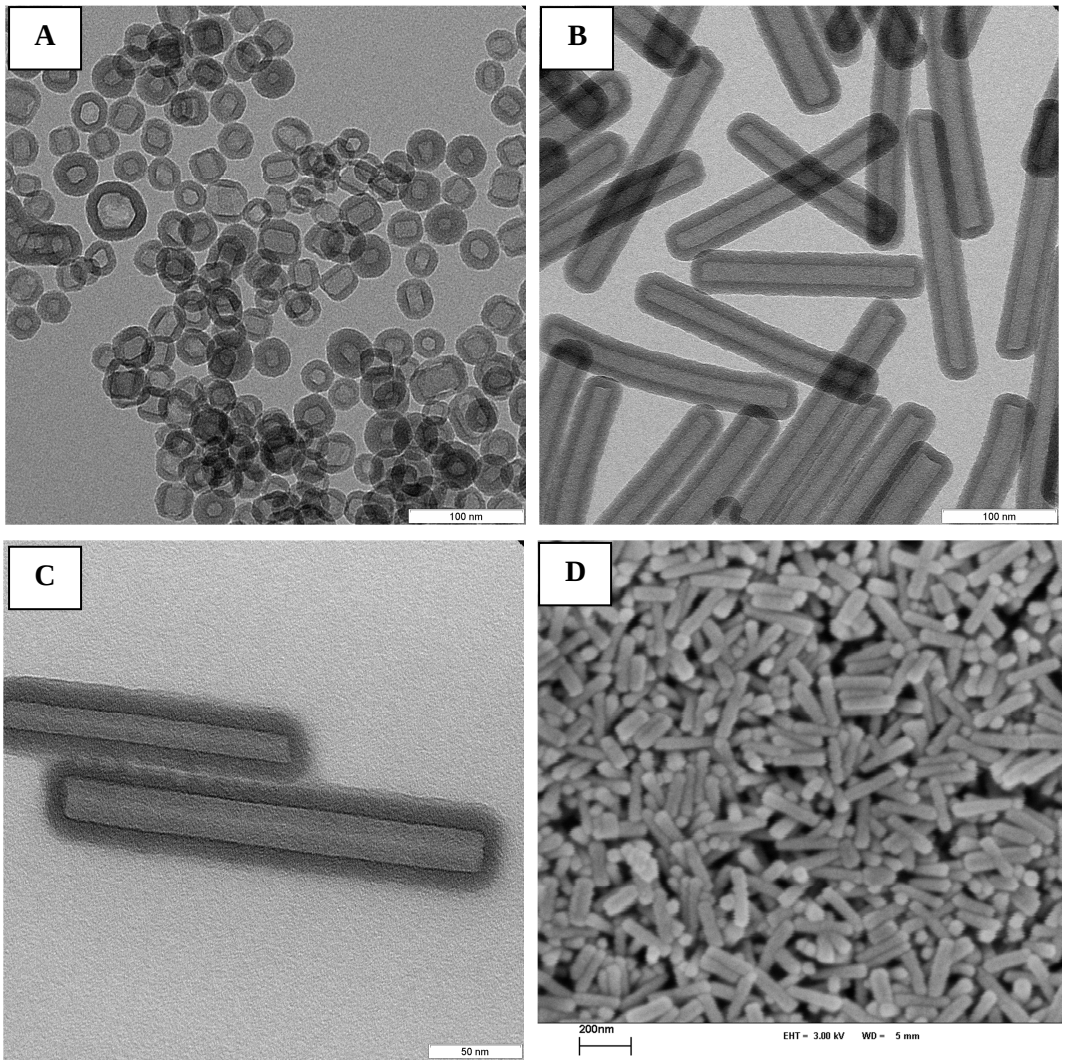

Figure 2 TEM images of the silica nanotubes with aspect ratio of (A) 1.16 and (B) 5.02; TEM (C) and SEM (D) images of the silica-*g*-(PLA-*b*-PEG) hybrid nanotubes with aspect ratio of 4.72. The scale bars are 100, 100, 50, and 200 nm, respectively.

Table 1 Physiochemical properties of the PLA-*b*-PEG diblock copolymer-decorated anisotropic silica nanotubes.

Entry[a]	**NT1**[b]	**NT2**	**NT3**	**NT4**
L_n (nm)	43.8	45.2	211.5	216.3
D_n (nm)	37.9	40.2	42.1	45.8

d_n (nm)	10.1	11.0	12.1	13.7
Aspect Ratios (ARs, L_n/D_n)	1.16	1.12	5.02	4.72
Surface Functional Groups (F)	-COOH	-PLA-*b*-PEG	-COOH	-PLA-*b*-PEG
Cell Viability	49.4	56.2	63.8	71.1

[a] L_n: number-averaged length; D_n, d_n: number-averaged outer and thickness; L_n/D_n: aspect ratio; F: surface functional group. [b]The statistic data is from TEM images.

To confirm the formation of covalent decoration of PLA-*b*-PEG diblock copolymer on silica surfaces, Figure 3 shows the FT-IR spectra of the as-synthesized nanotubes before and after surface decoration of diblock copolymers. For the silica-COOH nanotubes, the absorption band at around 3320 cm^{-1} is associated with the -OH stretching region from the carboxylic acid groups on the silica surfaces prior to surface modification. For silica-*g*-(PLA-*b*-PEG) hybrid nanotubes, the new absorption peaks at 1750 cm^{-1} and 2881cm^{-1} are due to the characteristic stretching vibration of the -C=O groups from PLA segments and -C-H stretching bands of diblock copolymers.[41] As shown in Figure 4, the new chemical shifts of 5.18 ppm (peak 1) and 3.65 ppm (peak 2) in the ^{1}H NMR spectrum of the silica-*g*-(PLA-*b*-PEG) hybrid nanotubes corresponds to the protons from -CH- and -CH_2CH_2O- groups of PLA and PEG segment, respectively. The FT-IR and ^{1}H NMR spectra indicate that the silica nanotubes were decorated with PLA-*b*-PEG diblock copolymers. For the application of hybrid nanotubes in oral delivery, the outmost hydrophilic PEG segments of nanotubes can improve their solubility and protect against immune response, whereas the PLA segments can serve as a cleavable barrier once the nanotubes are delivered onto the targeting sites of tumors, because of the breakup of ester groups in acid environment.[42]

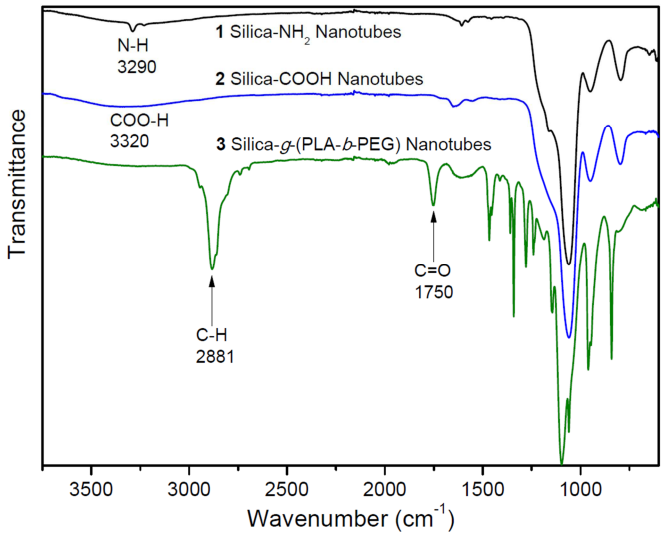

Figure 3 FT-IR spectra of the silica-NH_2, silica-COOH and silica-*g*-(PLA-*b*-PEG) nanotubes.

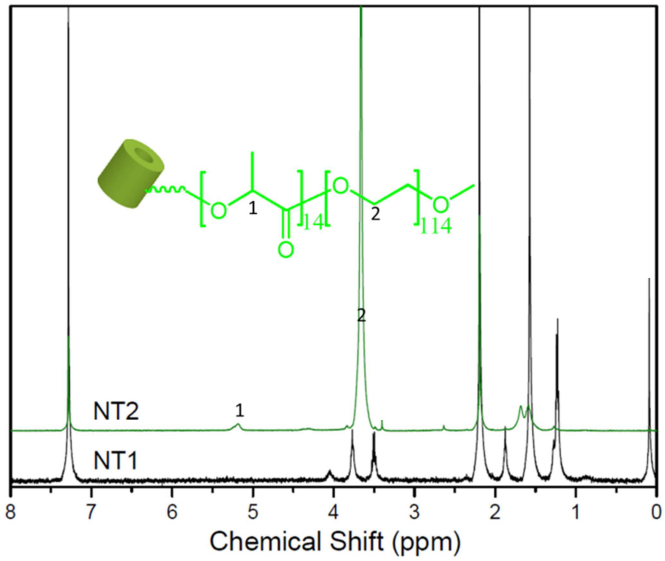

Figure 4 ^{1}H NMR spectra of the nanotubes in $CDCl_3$ before and after decoration of PLA-*b*-PEG diblock copolymers on surfaces.

The mesoporous structure of silica tubes was determined by Brunauer-Emmett-Teller (BET) adsorption-desorption isotherms (**Supporting Information, Figure S3 and Table S2**). The pores in the silica wall have an average diameter of 3.7 nm and volume of 1.1-1.4 cc/g. The grafting density of PLA-*block*-PEG chains on the surface of silica nanotubes was measured from the weight loss of polymer chains in the thermogravimetric analysis (TGA, Figure 5), and is calculated as 0.51 chains/nm^2. This surface grafting density is comparable to that reported in literature via the "grafting to" approach.[43, 44] The average spacing between neighboring chains then is approximately 1.4 nm much less than the diameter 3.7 nm of the

silica wall pores, ensuring that the PLA-*block*-PEG layer provides a physical barrier for the diffusion of drug molecules carried inside the nanotubes. The as-prepared silica-*g*-(PLA-*b*-PEG) hybrid nanotubes have a cavity of diameter around 10 nm for encapsulation, mesoporous silica inner wall for diffusion and amphiphilic PLA-*b*-PEG copolymer outer shell as biocompatible barrier layer for sustained release.

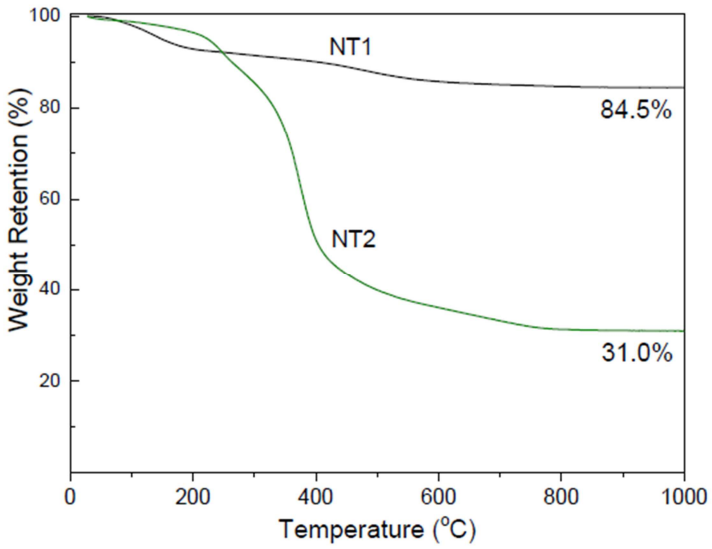

Figure 5 Thermogravimetric analysis (TGA) of the synthesized hybrid nanotubes at a heating rate of 10°C/min in N_2 (NT1 and NT2 are bare silica nanotubes and silica/polymer hybrid nanotubes, respectively).

As a preliminary application, the synthesized silica-COOH and silica-*g*-(PLA-*b*-PEG) nanotubes were tested for controlled drug release, where the fluorescent probe Rhodamine 6G was utilized as a model drug. The release curves from four kinds of nanotubes are shown in Figure 6. The free Rh6G molecules without encapsulation in nanotubes are rapidly released. The release curves from the two bare silica-COOH nanotubes (NT1 and NT3, without diblock copolymers on surfaces) are close and show about 90% release of Rh6G within 24 hours. However, a sustained release dynamics of Rh6G was observed for the silica-*g*-(PLA-*b*-PEG) hybrid nanotubes (NT2 and NT4). In contrast to that of bare silica-COOH nanotubes (NT1 and NT3), the release percentage of Rh6G from NT4 is reduced to around 40% over 48 hours. It indicates that the PLA-*b*-PEG diblock chains provide a physical barrier for the diffusion of

Rh6G, Meanwhile, the Rh6G molecules in longer NT4 nanotubes show a slower release than in NT2.

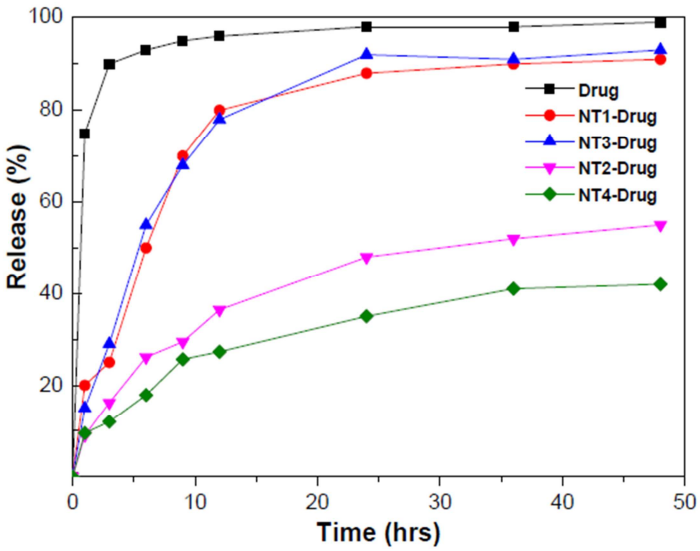

Figure 6 Release dynamics of rhodamine 6G from the as-synthesized nanocontainers (NT1 and NT3 are bare silica nanotubes, NT2 and NT4 are hybrid nanotubes with diblock copolymers on surface, respectively).

The cytotoxicity of the synthesized nanotubes was further evaluated for NIH 3T3 fibroblast cells. The outer diameter of all prepared nanotubes is around 40 nm, much larger than the cell-membrane thickness of about 5 nm, whereas the diameter of protein channel in cell membranes is up to 3 nm, [45, 46] implying that cellular uptake of the nanotubes occurs via endocytosis instead of translocation across membranes. The synthesized four types of nanotubes were incubated with NIH 3T3 cells for 48 hours with the same concentration of 100 μg/mL. In Figure 7, the cellular cytotoxicity depends on the nanocontainer shape and surface properties.[26, 47, 48] The nanotubes with higher aspect ratio lead to higher cell viability and thus lower cytotoxicity (NT1 vs. NT3, NT2 vs. NT4). The anisotropic nanotubes decorated with amphiphilic diblock copolymers (NT4) exhibit the lowest cellular cytotoxicity.

To understand the cellular cytotoxicity results, the free energy cost for fully wrapping a nanoparticle by cell membranes, which consists of bending and stretching energy E_{be} and E_{st}

from membrane elastic deformation,[49] and adhesion energy ε_{ad} between the membrane and nanoparticle is calculated:

$$\Delta G = E_{be} + E_{st} + \varepsilon_{ad} = 2\kappa \oint (\bar{c} - c_0)^2 dA + \gamma A - \varepsilon_{ad} A \qquad (1)$$

Where κ is the membrane bending modulus, $\bar{c}$ and c_0 the mean and spontaneous curvature, γ the membrane surface tension, A the nanoparticle area and ε_{ad} the adhesion strength.

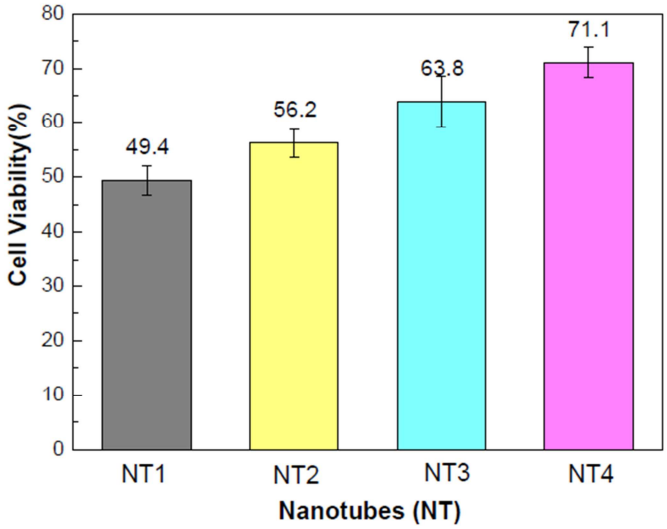

Figure 7 Viability test of NIH 3T3 fibroblast cells incubated for 48 hours with the four types of nanocontainer at the same concentration of 100 μg/mL.

For NIH 3T3 cell membranes, $\kappa = 3.0 \times 10^{-19}$ J, $\gamma = 5.9 \times 10^{-5}$ N/m from experiments[50] and we assume $c_0 = 0$. The probability p to fully wrap a nanoparticle is proportional to the Boltzmann weight $e^{-\Delta G/kBT}$ with $k_B T$ the thermal energy. In the cytotoxicity experiments n cells are interacting with the same weight of nanoparticles (particle number N), and the probability to cause the death of a cell might be related to the number of nanoparticles it encapsulates via

$$1\text{-}v = f\,(pN/n) \qquad (2)$$

Where v is the cell viability and pN/n is the average number of fully-wrapped nanoparticles per cell. The function f generally increases with pN/n, while its exact form might be cell specific.

As shown in Figure 7, the bare silica nanotube ("b") and its hybrid counterpart with polymer grafting ("h"), which have the same geometry but different surface properties, yield nearly the same cell viability v, implying $p_b N_b \approx p_h N_h$. The TGA data in Figure 5 reveals a weight percentage of 63% for the polymer shell on the container surfacess, so $N_h/N_b = 0.37$. Our physical argument leads to $p_b/p_h \approx 0.37$ and thus $\Delta G_b \approx \Delta G_h + k_B T$, suggesting that the polymer decoration slightly increases the adhesion strength ε_{ad}. Figure 7 also shows that longer nanoparticles ("l") lead to greater v than shorter ones ("s") with the same surface chemistry, i.e., $p_l N_l < p_s N_s$. According to the geometry data in Table 1, $N_s/N_l \approx 6$, which gives $p_l/p_s < 6$. As a crude approximation, the nanotube is considered as a spherocylinder of total length L and diameter D, for which $E_{be} = 2\pi\kappa\ (L/D + 3)$ and $E_{st} + \varepsilon_{ad} = \pi LD\ (\gamma - E_{ad})$. At $\varepsilon_{ad} = \varepsilon_{ad}^{c} \equiv 2\kappa\ (L/D+3)/(LD)+\gamma$, $\Delta G = 0$. We obtain $\varepsilon_{ad}^{c} \approx 1.5 \times 10^{-3}$ N/m for the NT1 and NT2 nanotubes, and $\varepsilon_c \approx 6 \times 10^{-4}$ N/m for NT3 and NT4, both larger than the strength 4.1×10^{-4} N/m of HIV virus binding to a cell membrane.[51] It is reasonable to assume $\varepsilon_{ad} < \varepsilon_{ad}^{c}$ for our nanotubes. In this case, $\Delta G > 0$ increases with length L, so $p_l < p_s$, which is consistent with our prediction of $p_l/p_s < 6$ obtained from the viability data.

Conclusions

A synthetic strategy of amphiphilic diblock copolymer-decorated anisotropic silica nanotubes which integrated anisotropic shape and surface property has been demonstrated. The surface decoration of PLA-*b*-PEG diblock copolymers on anisotropic silica nanotubes can reduce the leakage of active molecules from the bare silica containers. It is due to the barrier effect of grated polymers on container surfaces. The anisotropic container with high aspect ratio and diblock copolymer decoration on surfaces shows improved/enhanced activities from the sustained release and 3T3 fibroblast cellular cytotoxicity test. This study shows the importance of integrating anisotropic shape and surface property in one nanocontainer, which provides a comprehensive view for future sophisticated container/vehicles design in complex biological systems. The optimized nanocontainers will serve as promising building blocks for

oral delivery and cancer research.

Acknowledgements

G. Li. acknowledges support by the One Hundred Talent Program of Chinese Academy of Sciences, as well as by the Alexander von Humboldt fellowship. D. S. thanks ERC Consolidator Grant “Enercapsule”. We thank Ms. Rona Pitschke for TEM, Dr. Ran Yu for ^{1}H NMR, Dr. Matthias Schenderlein for TGA measurements.

Supporting Information

The supporting Information is available free of charge on the ACS Publications website: The FT-IR spectra, ^{1}H NMR spectra, UV-Vis absorption spectra, and BET N_2 adsorption-desorption isotherm of silica/polymer hybrid nanotubes.

References and Notes

[1] C.E. Diesendruck, N.R. Sottos, J.S. Moore, S.R. White, Angew Chem Int Edit, 54 (2015) 10428-10447.
[2] W. Meier, Chem Soc Rev, 29 (2000) 295-303.
[3] M. Gragert, M. Schunack, W.H. Binder, Macromol Rapid Comm, 32 (2011) 419-425.
[4] Z.Y. Wang, L. Zhou, X.W. Lou, Adv Mater, 24 (2012) 1903-1911.
[5] J. Gaitzsch, X. Huang, B. Voit, Chemical Reviews, 116 (2016) 1053-1093.
[6] K.T. Kim, S.A. Meeuwissen, R.J.M. Nolte, J.C.M. van Hest, Nanoscale, 2 (2010) 844-858.
[7] D. Peer, J.M. Karp, S. Hong, O.C. FaroKHzad, R. Margalit, R. Langer, Nat Nanotechnol, 2 (2007) 751-760.
[8] R. Duncan, Nature Reviews Drug Discovery, 2 (2003) 347-360.
[9] K. Liu, R.R. Xing, Q.L. Zou, G.H. Ma, H. Mohwald, X.H. Yan, Angew Chem Int Edit, 55 (2016) 3036-3039.
[10] A.R. Studart, Angew Chem Int Edit, 54 (2015) 3400-3416.
[11] J. Fothergill, M. Li, S.A. Davis, J.A. Cunningham, S. Mann, Langmuir, 30 (2014) 14591-14596.
[12] J.J. Shi, A.R. Votruba, O.C. Farokhzad, R. Langer, Nano Letters, 10 (2010) 3223-3230.
[13] P. Zhao, L.X. Liu, X.Q. Feng, C. Wang, X.T. Shuai, Y.M. Chen, Macromol Rapid Comm, 33 (2012) 1351-1355.
[14] J. Wang, K. Liu, R.R. Xing, X.H. Yan, Chem Soc Rev, 45 (2016) 5589-5604.
[15] S. Bai, C. Pappas, S. Debnath, P.W.J.M. Frederix, J. Leckie, S. Fleming, R.V. Ulijn, Acs Nano, 8 (2014) 7005-7013.
[16] D. Huhn, K. Kantner, C. Geidel, S. Brandholt, I. De Cock, S.J.H. Soenen, P.R. Gil, J.M. Montenegro, K. Braeckmans, K. Mullen, G.U. Nienhaus, M. Klapper, W.J. Parak, Acs Nano, 7 (2013) 3253-3263.
[17] N.W. Li, W.H. Binder, Journal of Materials Chemistry, 21 (2011) 16717-16734.
[18] W.O. Yah, A. Takahara, Y.M. Lvov, Journal of the American Chemical Society, 134 (2012) 1853-1859.

[19] M. Qi, S. Duan, B.R. Yu, H. Yao, W. Tian, F.J. Xu, Polymer Chemistry, 7 (2016) 4334-4341.
[20] L.Q. Xu, D. Pranantyo, Y.X. Ng, S.L.M. Teo, K.G. Neoh, E.T. Kang, G.D. Fu, Industrial & Engineering Chemistry Research, 54 (2015) 5959-5967.
[21] C. Huang, K.G. Neoh, E.T. Kang, Langmuir, 28 (2012) 563-571.
[22] W. Wei, D. Zhu, Z.H. Wang, D.Z. Ni, H. Yue, S. Wang, Y. Tao, G.H. Ma, Journal of Materials Chemistry B, 4 (2016) 2548-2552.
[23] X.L. Feng, F.T. Lv, L.B. Liu, H.W. Tang, C.F. Xing, Q.O. Yang, S. Wang, Acs Appl Mater Inter, 2 (2010) 2429-2435.
[24] J.L. Perry, K.P. Herlihy, M.E. Napier, J.M. Desimone, Accounts of Chemical Research, 44 (2011) 990-998.
[25] M.G. Soliman, B. Pelaz, W.J. Parak, P. del Pino, Chemistry of Materials, 27 (2015) 990-997.
[26] T. Yu, A. Malugin, H. Ghandehari, Acs Nano, 5 (2011) 5717-5728.
[27] Y. Geng, P. Dalhaimer, S.S. Cai, R. Tsai, M. Tewari, T. Minko, D.E. Discher, Nat Nanotechnol, 2 (2007) 249-255.
[28] Y. Lu, D.L. Slomberg, B. Sun, M.H. Schoenfisch, Small, 9 (2013) 2189-2198.
[29] Y. Hu, Y.Q. Zhou, N.N. Zhao, F.S. Liu, F.J. Xu, Small, 12 (2016) 2459-2468.
[30] F. Gentile, C. Chiappini, D. Fine, R.C. Bhavane, M.S. Peluccio, M.M.C. Cheng, X. Liu, M. Ferrari, P. Decuzzi, J Biomech, 41 (2008) 2312-2318.
[31] J. Wang, W. Zhu, L.X. Liu, Y.M. Chen, C. Wang, Acs Appl Mater Inter, 7 (2015) 5454-5461.
[32] A. Nazemi, C.E. Boott, D.J. Lunn, J. Gwyther, D.W. Hayward, R.M. Richardson, M.A. Winnik, I. Manners, Journal of the American Chemical Society, 138 (2016) 4484-4493.
[33] J. Qian, Y. Lu, A. Chia, M. Zhang, P.A. Rupar, N. Gunari, G.C. Walker, G. Cambridge, F. He, G. Guerin, I. Manners, M.A. Winnik, Acs Nano, 7 (2013) 3754-3766.
[34] M.S. Hsiao, S.F.M. Yusoff, M.A. Winnik, I. Manners, Macromolecules, 47 (2014) 2361-2372.
[35] H. Zhou, Y.J. Lu, M. Zhang, G. Guerin, I. Manners, M.A. Winnik, Macromolecules, 49 (2016) 4265-4276.
[36] S. Biswas, K. Kinbara, T. Niwa, H. Taguchi, N. Ishii, S. Watanabe, K. Miyata, K. Kataoka, T. Aida, Nature Chemistry, 5 (2013) 613-620.
[37] C.B. Gao, Z.D. Lu, Y.D. Yin, Langmuir, 27 (2011) 12201-12208.
[38] G.L. Li, Z.L. Zheng, H. Mohwald, D.G. Shchukin, Acs Nano, 7 (2013) 2470-2478.
[39] Y.Q. An, M. Chen, Q.J. Xue, W.M. Liu, Journal of Colloid and Interface Science, 311 (2007) 507-513.
[40] H.J. Salavagione, M.A. Gomez, G. Martinez, Macromolecules, 42 (2009) 6331-6334.
[41] K. Jelonek, S.M. Li, B. Kaczmarczyk, A. Marcinkowski, A. Orchel, M. Musial-Kulik, J. Kasperczyk, Int J Pharmaceut, 510 (2016) 365-374.
[42] J. Palacio, N.A. Agudelo, B.L. Lopez, Curr Opin Chem Eng, 11 (2016) 14-19.
[43] C. Tonhauser, A.A. Golriz, C. Moers, R. Klein, H.J. Butt, H. Frey, Adv Mater, 24 (2012) 5559-5563.
[44] G.L. Li, D. Wan, K.G. Neoh, E.T. Kang, Macromolecules, 43 (2010) 10275-10282.
[45] B. Alberts, Molecular biology of the cell, Sixth edition. ed.
[46] F. Bonardi, E. Halza, M. Walko, F. Du Plessis, N. Nouwen, B.L. Feringa, A.J.M. Driessen, P Natl Acad Sci USA, 108 (2011) 7775-7780.
[47] K. Ariga, J.B. Li, J.B. Fei, Q.M. Ji, J.P. Hill, Adv Mater, 28 (2016) 1251-1286.
[48] C.L. Du, J. Zhao, J.B. Fei, Y. Cui, J.B. Li, Advanced Healthcare Materials, 2 (2013) 1246-1251.
[49] W. Helfrich, Zeitschrift Fur Naturforschung C-a Journal of Biosciences, C 28 (1973) 693-703.

[50] B. Pontes, N.B. Viana, L.T. Salgado, M. Farina, V.M. Neto, H.M. Nussenzveig, Biophysical Journal, 101 (2011) 43-52.
[51] S.X. Sun, D. Wirtz, Biophysical Journal, 90 (2006) L10-L12.